Effect of the Insulating Shield Thickness on the Steady-State Diffusion-Limiting Current of Sphere Cap Microelectrodes

ARTICLE *in* ANALYTICAL CHEMISTRY · FEBRUARY 2008

Impact Factor: 5.64 · DOI: 10.1021/ac701631y · Source: PubMed

3 AUTHORS, INCLUDING:

S. Daniele
Università Ca' Foscari Venezia
138 PUBLICATIONS **2,052** CITATIONS
SEE PROFILE

Dario Battistel
Università Ca' Foscari Venezia
25 PUBLICATIONS **208** CITATIONS
SEE PROFILE

Anal. Chem. **2008,** *80,* 253−259

Effect of the Insulating Shield Thickness on the Steady-State Diffusion-Limiting Current of Sphere Cap Microelectrodes

Salvatore Daniele,* Ilenia Ciani,† and Dario Battistel

Department of Physical Chemistry, University of Venice, Calle Larga, S. Marta, 2137, 30123 Venice, Italy

The effect of the insulating shield thickness on the steady-state diffusion-limiting current of sphere cap microelectrodes is investigated. Theoretical steady-state limiting currents are obtained by using a simulation procedure, which relies on the explicit finite difference method with a fixed time grid and an exponentially spatial grid. The results obtained indicate that the current increases by decreasing the thickness of the insulating sheath or by increasing the aspect ratio of the sphere cap (*h*/*a*, where *h* is the height of the sphere cap and *a* is the electrode basal radius), similarly to other types of microelectrodes with different electrode geometry, such as disks and finite cones. The simulated data are fitted to approximate analytical expressions to describe the dependence of the limiting current on both *h*/*a* and *RG* (*RG* = *b*/*a*, where *b* is the overall tip radius) parameter. Theoretical currents are also compared with experimental data, which are obtained with a range of mercury-coated platinum microelectrodes having different *RG* and *h*/*a* values. The measurements are performed by using cyclic voltammetry at 1 mVs^{-1}, in aqueous solutions containing $Ru(NH_3)_6Cl_3$ as electroactive species. A good agreement (within 3%) between theoretical and experimental steady-state currents is found. Finally, SECM operating in the feedback mode is used to assess the validity of the shape parameters found by voltammetry for sphere cap microelectrodes, whose insulating shields are of a thickness comparable to the electrode radius.

Microelectrodes[1−4] with geometry different from the commonest disk shape have becoming more popular recently.[5−17] Finite conical[5−9] and spherical microelectrodes,[9−15] in particular, have found increasing interest because they can be used as tips in scanning electrochemical microscopy (SECM).[18−22] The microelectrode shape and the overall tip dimension, which includes the active surface area and the surrounding insulator, affect the current responses, and theory for both the above types of electrode geometry have been developed within the SECM configuration.[6,10,11,13,15,19,20,21] In particular, theoretical analyses exist for the microtips approaching either a conducting or an insulating surface. In these cases, only normalized currents (i.e., the ratio of the current at a given tip−surface distance to that in the bulk solution) are required. Theory for predicting the diffusion-limited steady-state current for finite cones and sphere caps has also been developed. For finite conical microtips, approximate analytical expressions have been reported to describe the dependence of the steady-state current on both the aspect ratio and the thickness of the insulating sheath.[5,6] For sphere cap microelectrodes, equations for steady-state limiting current have also been reported, but they were limited to the special case of sphere caps that rest on an infinite insulating plane.[23,24] It is known that a thinner insulating sheath produces an enhanced flux to the electrode surface, because of diffusion of the electroactive species from

* To whom correspondence should be addressed. E-mail: sig@unive.it. Tel.: + 390412348630. Fax: + 390412348594.

† Current address: School of Chemistry, University of Edinburgh, EH9 3JJ, Edinburgh, UK.

(1) Wightmann, R. M.; Wipf, D. O. In *Electroanalytical Chemistry*; Bard, A. J., Ed.; Marcel Dekker: New York, 1989; Vol. 15, pp 267−353.
(2) *Microelectrodes: Theory and Applications*; Montenegro, M. I., Queiros, M. A., Daschbach, J. L., Eds.; NATO ASI Series; Kluwer Academic Publishers: Dordrecht, The Netherlands, 1991.
(3) Zoski, C. G. *Electroanalysis* **2002**, *14*, 1041−1051.
(4) Arrigan, D. W. M. *Analyst* **2004**, *129*, 1157−1165.
(5) Zoski, C. G.; Mirkin, M. V. *Anal. Chem.* **2002**, *74*, 1986−1992.
(6) Zoski, C. G.; Liu, B.; Bard, A. J. *Anal. Chem.* **2004**, *76*, 3646−3654.
(7) Jones, C. E.; Unwin, P. R.; Macpherson, J. V. *Chem. Phys. Chem.* **2003**, *4*, 139−146.
(8) Sklyar, O.; Kueng, A.; Kranz, C.; Mizaikoff, B.; Lugstein, A.; Emmerich, B.; Bertagnolli, E.; Wittstock, G. *Anal. Chem.* **2005**, *7*, 764−771.
(9) Machpherson, J. V.; Unwin, P. R. *Anal. Chem.* **2000**, *72*, 276−285.
(10) Selzer, Y.; Mandler, D. *Anal. Chem.* **2000**, *72*, 2383−2390.
(11) Demaille, C.; Brust, M. B.; Tsionsky, M.; Bard, A. J. *Anal. Chem.* **1997**, *69*, 2323−2328.
(12) Abbou, J.; Demaille, C.; Druet, M.; Moiroux J. *Anal. Chem.* **2002**, *74*, 6355−6363.
(13) Daniele, S.; Bragato, C.; Ciani, I.; Baldo, M. A. *Electroanalysis* **2003**, *15*, 621−627.
(14) Ciani, I.; Daniele, S.; Bragato, C.; Baldo, M. A. *Electrochem. Commun.* **2003**, *5*, 354−358.
(15) Lindsey, G.; Abercrombie, S.; Denuault, G.; Daniele, S.; De Faveri, E. *Anal. Chem.* **2007**, *79*, 2952−2956.
(16) Lee, Y.; Amemiya, S.; Bard, A. J. *Anal. Chem.* **2001**, *73*, 2261−2267.
(17) Liljeroth, P.; Johans, C.; Slevin, C. J.; Quinn, B. M.; Kontturi, K. *Anal. Chem.* **2002**, *74*, 1972−1978.
(18) Bard, A. J., Mirkin, M. V., Eds. *Scanning Electrochemical Microscopy*; Marcel Dekker, Inc.: New York, 2001.
(19) Fulian, Q.; Fisher, A. C.; Denuault, G. *J. Phys. Chem. B* **1999**, *103*, 4387−4392.
(20) Fulian, Q.; Fisher, A. C.; Denuault, G. *J. Phys. Chem. B* **1999**, *103*, 4393−4398.
(21) Peng, S.; Laforge, F. O.; Mirkin, M. V. *Phys. Chem. Chem. Phys.* **2007**, *9*, 802−823.
(22) Wittstock, G.; Burchart, M.; Pust, S. E.; Shen, Y.; Zhao, C. *Angew. Chem., Int. Ed.* **2007**, *46*, 1584−1617.
(23) Myland, J. C.; Oldham, K. B. *J. Electroanal. Chem.* **1990**, *288*, 1 14.
(24) Alfred, L. C. R.; Oldham, K. B. *J. Phys. Chem.* **1996**, *100*, 2170−2177.

10.1021/ac701631y CCC: $40.75
Published on Web 12/06/2007

behind the plane of the electrode. This has been demonstrated and quantified for both an inlaid microdisk[25−32] and a finite microcone,[5,6] whereas for a sphere cap there is no report that provides quantitative analysis of the effect of back diffusion to the steady-state limiting current specifically.

From a practical point of view, sphere cap microelectrodes are usually prepared by electrodeposition of mercury onto microdisk electrodes of materials that are wettable by mercury, such as Pt,[33−36] Au,[37,38] Ir,[39,40] and Ag.[41] These electrodes have found widespread use in electroanalysis[13,42−45] and for kinetic measurements.[38,46] Despite the numerous reports on the preparation and application of mercury microelectrodes in various fields, only a few papers have dealt with the experimental performance of sphere cap microelectrodes with thickness of the insulating shield comparable to the electrode radius in voltammetric measurements.[15]

Aimed at addressing the above as yet unconsidered aspects, in this paper, we report on the steady-state limiting currents at sphere cap microelectrodes as a function of both the aspect ratio, h/a (where h is the height of the sphere cap and a is the basal disk radius) and insulating sheath thickness $RG = b/a$ (i.e., the ratio of the overall tip radius b, to the basal radius of the electrode a, Figure 1). Theoretical steady-state limiting currents are obtained by using the simulation procedure described in refs 28 and 32 for thin-shielded microdisks, which is adapted to the sphere cap geometry. Experimental data are obtained with a range of mercury-coated platinum microelectrodes having different RG and h/a values, in an aqueous solution containing $Ru(NH_3)_6Cl_3$ as electroactive species. Moreover, the various geometric parameters of thin-shielded mercury microelectrodes are also assessed by SECM operating in feedback mode.[18]

EXPERIMENTAL SECTION

Chemicals and Materials. All chemicals were of analytical grade and used as received. Ruthenium(III) hexaammine trichloride, potassium nitrate, potassium chloride, and nitric acid were purchased from Aldrich. Aqueous solutions were prepared using MilliQ water (Millipore, Bedford, MA). Cathodic electrophoresis paint Stollaquid D 1330 was supplied from Herberts. Before use, the paint was diluted 1:6 with MilliQ water and the resulting suspension was stirred for at least 24 h. Pt microwires (20 and 25 μm in diameter) were purchased from Goodfellow (Cambridge, England).

All voltammetric measurements requiring no oxygen were carried out in solutions that had been purged with pure nitrogen (99.99%) (from SIAD).

Electrodes. The platinum microdisks, which served as the substrate for mercury deposition, were prepared either by sealing wires of 10- and 12.5-μm radius into glass capillaries or by coating the cylindrical length of the Pt wires with a cathodic electrophoretic paint as described previously.[32,47] The latter procedure was employed to prepare Pt microdisk with very thin insulating shields (i.e., $RG = 1.3-2.1$). To expose the microdisk, the end part of the paint-insulated electrode was cut off with a microsurgical scalpel blade. Since this procedure may lead to the deformation of the Pt wire, the occurrence of a good sealing and a sufficiently round microdisk were ascertained by SEM inspection of the microelectrode tip end. Only those microtips that displayed the latter characteristics (success rate 20−30%) were used as substrate for mercury deposition. The thicker glass-coated electrode tips, which were sealed by standard procedures, were tapered to form a truncated conical shape, analogous to a conventional SECM tip.[18] Prior to mercury deposition, the glass-embedded microdisks were polished with graded alumina powder of different sizes (1, 0.3, and 0.05 μm) on a polishing microcloth. For each microdisk, the radius of the insulating sheath, as is customary, was determined with an optical microscope or by SEM while preparing the microtips. The values thus evaluated were further confirmed by fitting theoretical SECM approach curves[18] to experimental ones recorded under purely diffusion-controlled conditions. Moreover, for the thin-shielded microdisks, the cyclic voltammetric procedure described in ref 32 was also employed. Sphere cap mercury microelectrodes of different sizes were prepared by cathodic deposition of mercury onto the platinum microdisks.[36] The deposition was performed under potentiostatic conditions at −0.1 V against an Ag/AgCl reference electrode in a plating solution consisting of 5 mM $Hg_2(NO_3)_2$ in 1 M KNO_3

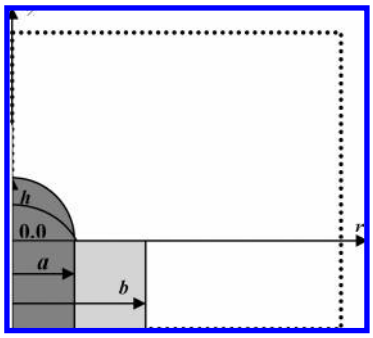

Figure 1. Schematic representation of a sphere cap and simulation domain.

(25) Ciani, I.; Daniele, S. *J. Electroanal. Chem.* **2004**, *564*, 133−140.
(26) Kwak, J.; Bard, A. J. *Anal. Chem.* **1989**, *61*, 1221−1227.
(27) Amphlett, J. L.; Denuault, G. *J. Phys. Chem. B* **1998**, *102*, 9946−9951.
(28) Fang Y.; Leddy, J. *Anal. Chem.* **1995**, *67*, 1259−1270.
(29) Zhao, G.; Giolando, D. M.; Kirchoff, J. R. *Anal. Chem.* **1995**, *67*, 2592−2598.
(30) Shoup, D.; Szabo, A. *J. Electroanal. Chem.* **1982**, *140*, 237−245.
(31) Shoup, D.; Szabo, A. *J. Electroanal. Chem.* **1984**, *160*, 27−31.
(32) Ciani, I.; Daniele, S. *Anal. Chem.* **2004**, *76*, 6575−6581.
(33) Wehmeyer, K. R.; Wightman, R. M. *Anal. Chem.* **1985**, *57*, 1989−1993.
(34) Stojek, Z.; Osteryoung, J. *Anal. Chem.* **1989**, *66*, 1305−1308.
(35) Colyer, C. L.; Luscombe, D.; Oldham, K. B. *J. Electroanal. Chem.* **1990**, *283*, 379−387.
(36) Daniele, S.; Bragato, C.; Baldo, M. A.; Mazzocchin, G. A. *Ann. Chim. (Rome)* **2002**, *92*, 203−215.
(37) Baranski, A. S.; Quon, H. *Anal. Chem.* **1986**, *58*, 407−412.
(38) Birke, R. L.; Huang, Z. *Anal. Chem.* **1992**, *64*, 1513−1520.
(39) Golas, J.; Galus, Z.; Osteryoung, J. *Anal. Chem.* **1987**, *59*, 389−392.
(40) Kounaves, S. P.; Buffle, J. *J. Electroanal. Chem.* **1987**, *216*, 53−69.
(41) Ciszkowska, M.; Donten, M.; Stojek, Z. *Anal. Chem.* **1994**, *66*, 4112−4115.
(42) Baldo, M. A.; Daniele, S.; Ciani, I.; Bragato, C.; Wang, J. *Electroanalysis* **2004**, *5*, 360−365.
(43) Rudolph, D.; Neuhuber, S.; Kranz, C.; Taillefert, M.; Mizaikoff, B. *Analyst* **2004**, *129*, 443−448.
(44) Janotta, M.; Rudolph, D.; Kueng, A.; Kranz, C.; Voraberger, H. S.; Waldhauser, W.; Mizaikoff, B. *Langmuir* **2004**, *20*, 8634−8640.
(45) Economou, A.; Fielden, P. R. *Analyst* **2003**, *128*, 205−212.
(46) Correia dos Santos, M. M.; Vilhena, M. L.; Goncalves, S. *Anal. Chim. Acta* **2001**, *441*, 191−200.
(47) Zhang, X.; Ogorevc, B.; Rupnik, M.; Kreft, M.; Zorec, R. *Anal. Chim. Acta* **1999**, *378*, 135−143.

acidified with nitric acid to pH <1. Increasing deposition times were employed to obtain mercury deposits of different heights. The sphere cap height h was calculated from the sphere cap volume (V) given by[34,36,48] $V = \pi h(3a^2 + h^2)/6$ itself determined from the charge Q ($Q = V\rho F/M$, where ρ and M are the density and molar mass of mercury, respectively)[35] passed during the electrodeposition.

Apparatus. Cyclic voltammetry (CV) and chronoamperometric experiments were performed using an M 283 potentiostat/galvanostat (EG & PAR, Princeton, NJ) and the M 270 electrochemical software (EG&G PAR). The SECM micropositioning device consisted of a set of three stepper motor stages with a 0.1-μm resolution (Micos) with optical encoder (Zeiss), and the motion was controlled by a closed-loop motion controller board PCI-7324 (National Instruments). The data acquisition was performed by a PCI-6035E Multifunction I/O board controlled with Lab View (National Instruments). A CH700B workstation (CH Instruments) was employed for SECM measurements. The experiments were performed at room temperature (22 ± 1 °C), in a one-compartment electrochemical cell placed in an aluminum Faraday cage, using a two-electrode cell configuration.

RESULTS AND DISCUSSION

Simulation Model. The simulation model relies on the explicit finite difference algorithm, as described in detail elsewhere[28,32] (See also Supporting Information). The geometry of a sphere cap is described by the sphere cap basal disk of radius a, the height h, and the insulator thickness $b - a$ (Figure 1). The model was developed for a reversible heterogeneous electron-transfer reaction and assuming that mass transport is controlled by diffusion only. The steady-state diffusion equation in cylindrical coordinate is

$$D\left[\frac{\partial^2 c(r,z,t)}{\partial r^2} + \frac{1}{r}\frac{\partial c(r,z,t)}{\partial r} + \frac{\partial^2 c(r,z,t)}{\partial z^2}\right] = 0$$

where r and z are the coordinates in directions parallel and normal to the electrode base plane, respectively (see Figure 1), t is the time, $c(r,z,t)$ is the concentration, and D is the diffusion coefficient of both the oxidized and reduced species.

The boundary conditions were chosen in the standard way,[28,32] i.e., at the far edges of the simulation domain, defined by $r = r_{max}$ and $z = z_{max}$, the concentration was set equal to the bulk concentration; on the microelectrode surface, the concentration was imposed to be equal to zero, while all other surfaces were considered as insulating (i.e., zero flux). Moreover, to simplify the calculations, in the theoretical treatment, the superhemisphere ($h/a > 1$) and subhemisphere-hemisphere ($h/a \leq 1$) cases were addressed separately (Figure S1, Table S1, and Table S2, Supporting Information).

Verification of Simulation Validity and Optimization of Main Simulation Parameters. Preliminarily, the accuracy of the simulation code adopted here was tested against the steady-state limiting current expected for a hemispherical microelectrode (i.e., $h/a = 1$) and for a family of sphere caps protruding above an infinite insulating plane (i.e., $RG \rightarrow \infty$), for which analytical solutions exist.[1,2,23] The simulated steady-state limiting current (i) was normalized by the steady-state limiting current at an inlaid microdisk with $RG \rightarrow \infty$ ($i_{disk} = 4nFDc^b a$)[49] of identical basal radius (a):

$$I_{ss} = \frac{i}{4nFDc^b a} \quad (1)$$

where I_{ss} is the normalized steady-state limiting current, n is the number of electrons, F is the Faraday constant, and D and c^b are the diffusion coefficient and bulk concentration of the electroactive species, respectively.

Crucial parameters of the simulation are as follows: the number of grid elements across the electrode, N_a; the total number of grid elements along r, N_r, and along z, N_z; and the exponential factor that defines the rate of the grid spatial expansion, β (Supporting Information). An iterative process was used to optimize these parameters, which were varied one at a time to obtain the smallest difference (in any case below 1%) between simulated and expected current values. On the basis of previous works,[28,32] initially, a lattice $N_r \times N_z$ of 300 × 300 grid elements, and $\beta = 0.2$ were considered; N_a was then increased up to obtain values within the error tolerance. Once N_a was chosen, further sets of simulations were performed to optimize other parameters. From the simulations, it was verified that the current responses were affected mainly by N_a and β. As an example, Table 1 shows how the simulation outputs vary by changing the latter parameters for a hemisphere, for which the expected normalized current is equal to 1.5708. For $N_a = 30$ and $\beta = 0.05$, the simulated current equaled the expected value within 0.19%. As for N_r and N_z values, in general, a lattice of $N_r \times N_z$ of 300 × 300 grid elements, which was in turn optimized, proved good enough to provide accurate simulation outputs. In fact, setting $N_a = 30$ and $\beta = 0.05$, a further increase of both N_r and N_z did not provide any appreciable current change (i.e., ≪0.5%) with respect to that shown in Table 1 (fourth row). These optimized parameters were also employed to simulate steady-state diffusion-limiting currents for the family of sphere caps with aspect ratios in the range $0 \leq h/a \leq 2$ (which is the range of practical interest), and $RG \rightarrow \infty$. Table 2 shows simulated currents and for comparison those calculated by the analytical expression (eq 10) reported in ref 23. It is evident that our simulated results agree well (within 0.3%) with previous data.

The above optimized N_a parameter proved however insufficient to simulate diffusion-limiting currents for thin shielded sphere caps (TSSCs). In fact, for the latter cases, a series of simulations run

Table 1. Optimized Parameters in the Simulation of the Steady-State Current of a Hemisphere in an Infinite Insulating Plane

N_a	β	I_{ss}	ϵ, %
30	0.2	1.5106	3.8
30	0.1	1.5341	2.3
30	0.05	1.5680	0.18
25	0.05	1.5591	0.74
8	0.05	1.4641	6.8

(48) Baldo, M. A.; Daniele, S.; Corbetta, M.; Mazzocchin, G. A. *Electroanalysis* **1995**, *7*, 980−986.

(49) Saito, Y. *Rev. Polarogr.* **1968**, *15*, 177.

Table 2. Normalized Steady-State Current at Sphere Cap Microelectrodes for Different Values of *h/a* and *RG* → ∞[a]

h/a	$I_{ss(sim)}$	$I_{ss(th)}$	ϵ, %
0.00	1.002	1.000	0.20
0.10	1.036	1.034	0.19
0.22	1.085	1.082	0.28
0.54	1.251	1.249	0.16
0.86	1.468	1.464	0.27
1.00	1.568	1.571	0.19
1.14	1.687	1.684	0.18
1.50	1.999	1.996	0.15
1.81	2.287	2.283	0.18
2.00	2.469	2.464	0.20

[a] (sim) simulated and (th) calculated by eq 10 in ref 23; ϵ, %, error, %.

Table 3. Normalized Steady-State Currents for Different Values of *h/a* and *RG*

	h/a =						
RG	0.00	0.10	*0.54*	1.00	1.14	1.50	2.00
50.80	1.003	1.030	1.245	1.563	1.679	1.983	2.467
10.80	1.020	1.039	1.263	1.595	1.705	2.023	2.499
6.06	1.035	1.058	1.285	1.640	1.750	2.035	2.523
4.02	1.053	1.076	1.318	1.690	1.783	2.115	2.669
2.01	1.113	1.135	1.409	1.845	2.019	2.415	3.122
1.78	1.138	1.159	1.453	1.900	2.080	2.498	3.207
1.61	1.158	1.182	1.490	1.953	2.135	2.565	3.281
1.51	1.170	1.198	1.511	1.998	2.170	2.623	3.350
1.41	1.188	1.210	1.539	2.043	2.208	2.658	3.407
1.34	1.206	1.235	1.575	2.088	2.263	2.730	3.463
1.21	1.245	1.293	1.665	2.190	2.358	2.805	3.568
1.15	1.275	1.326	1.719	2.245	2.437	2.903	3.673
1.04	1.333	1.395	1.804	2.398	2.589	3.100	3.950

with increasing N_a indicated that the steady-state limiting currents converged to a constant value (within 1%) for $N_a \geq 30$ and depended on *RG*. In particular, for the thinnest family of TSSCs investigated here (i.e., $RG = 1.04$), $N_a = 70$ was required. Consequently, to simulate the steady-state limiting currents at various TSSCs with $RG \leq 50$ and $0 \leq h/a \leq 2$, the following parameters were chosen: $30 \leq N_a \leq 70$, $\beta = 0.05$, and $N_r = N_z = 300$. These parameters also proved accurate to simulate steady-state limiting currents for classical sphere caps (i.e., $RG \rightarrow \infty$). In fact, in all cases, I_{ss} values identical (within 0.3%) to those shown in Table 2 were found.

Results for TSSCs. Table 3 shows normalized, simulated steady-state diffusion-limiting currents for various values of *RG* and *h/a* (current data are also presented in graphical form in Figure S2 in the Supporting Information). As is evident, the current increases with decreasing *RG*, regardless of the sphere cap aspect ratio, analogously to disk and finite cone geometries.[5,6,16,25–32] The presence of the sphere cap significantly increases the steady-state current above that expected for the underlying microdisk. Moreover, simulated I_{ss} values for *RG* equal to 10 and 50 fit those found for the infinite insulator thickness within 2 and 0.8%, respectively (Tables 3 and 2). The normalized steady-state limiting currents of Table 3 can be described accurately (within 1%) by the analytical approximation:

$$I_{ss} = A + B(RG - C)^D \quad (2)$$

Table 4. Numerical Constants Corresponding to the Approximate Analytical Eq 2

	h/a =						
	0.00	0.10	0.54	1.00	1.14	1.50	2.00
A	1.0000	1.0344	1.2486	1.5708	1.6836	1.9956	2.4645
B	0.1445	0.1514	0.2723	0.4319	0.6607	1.6013	2.7727
C	0.6734	0.5727	0.4939	0.4927	0.2458	−0.2236	−0.4466
D	−0.8348	−1.1499	−1.2059	−1.0744	−1.3024	−1.7372	−1.7096

where *A*, *B*, *C*, and *D* are adjustable coefficients, which are collected in Table 4 for a range of *h/a* values. The form of eq 2 is similar to that used previously[5] for a disk and a finite cone geometry, and no attempt was made to have fewer adjustable coefficients. It must be noticed that the diffusion-limiting currents obtained by eq 2 for $h/a = 0$ (i.e., a microdisk) deviates slightly from those calculated by the similar equation reported in ref 5 (see also Figure 3 below), which further corroborates the validity of the simulation procedure employed here.

General Analytical Approximation. The objective of this section is to derive an approximated analytical expression that describes the steady-state diffusion-limiting current for microelectrodes with sphere cap geometries as a function of both *RG* and *h/a* parameters. The steady-state limiting current for a sphere cap (i_{Sc}) can be described by[23,34–36,38,48]

$$i_{Sc} = k_{Sc} nFDc^b a \quad (3)$$

where k_{Sc} is a "geometric" coefficient that depends on both *h/a* and *RG*, and the other symbols have their usual meanings. Thus, on the basis of eq 3, for a given experiment, the diffusion-limiting current can be predicted once k_{Sc} is known. In what follows, simulated data will be provided in terms of k_{Sc} values, which were evaluated by

$$k_{Sc} = 4I_{ss} \quad (4)$$

This way to interpret the results of the simulation was chosen because for the family of sphere caps with $RG \rightarrow \infty$, an analytical expression, relating the geometric coefficient $k_{RG\rightarrow\infty}$ and *h/a*, was provided (eq 11 in ref 23), and the graphical form of the latter equation is displayed in Figure 2 with a solid line. A very simple analytical approximation, which fits theoretical $k_{RG\rightarrow\infty}$ values (within 0.9%) was also derived and found to be of the form[36]

$$k_{RG\rightarrow\infty} = 4 + 2.2832(h/a)^{1.3590} \quad (5)$$

From this equation, it is evident that for $h/a = 0$, $k_{RG\rightarrow\infty} = 4$ (i.e, the coefficient for a microdisk).

From the simulated I_{ss} values, obtained for a given *RG* and different *h/a* values, a set of geometric coefficients, k_{RGi}, was calculated. Figure 2 includes k_{RGi} values (symbols) as a function of *h/a* for different *RG* values. Approximate relationships similar to eq 5 were also derived to describe k_{RGi} for each family of sphere caps that share a common *RG* value:

$$k_{RGi} = k_i + A_i(h/a)^{1.3590} \quad (6)$$

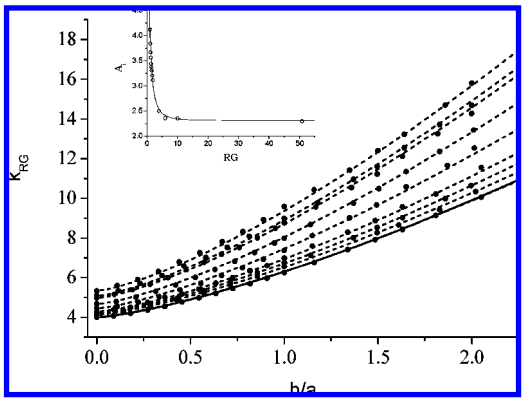

Figure 2. Simulated (symbols) values of k_{RGi} as a function of h/a for sphere cap microelectrodes having different values of RG, from top to the bottom RG = 1.04, 1.15, 1.21, 1.51, 1.78, 2.01, 3.0, 4.02, 6.06, and 50.80. The dashed lines represent the best fit through the series of points. The solid line represents the theoretical values calculated by eq 11 in ref 23 and refers to $RG \rightarrow \infty$. Inset: A_i as a function of RG; the solid line represents the best fit through the series of points.

where k_i and A_i are parameters that depend on RG. This equation was constructed by assuming that the power to h/a was equal to that found for $RG \rightarrow \infty$.

The functional dependence of k_i and A_i on RG was derived as follows. As for k_i, one may recognize that it actually accounts for the current dependence on RG of the underlying disk electrode onto which the sphere caps are grown. Therefore, from eq 2, specialized for $h/a = 0$ and I_{ss} multiplied by 4, one obtains

$$k_i = 4 + 0.5780(RG - 0.6734)^{-0.8348} \quad (7)$$

The parameter A_i, at each RG, was evaluated by fitting simulated k_{RGi} versus h/a, as shown in Figure 2 with dashed lines. The inset in Figure 2 shows A_i values (symbols) thus determined as a function of RG. These values, in turn, can be described by the following analytical approximation:

$$A = 2.2832 + 9.3279(RG + 1.0321)^{-2.2979} \quad (8)$$

The overall dependence of the of k_{Sc}, on both RG and h/a can therefore be described as

$$k_{Sc} = k_i + A(h/a)^{1.3590} \quad (9)$$

and after combining eqs 7−9, one obtains

$$k_{Sc} = (4 + 0.5780(RG - 0.6734)^{-0.8348}) + (2.2832 + 9.3279(RG + 1.0321)^{-2.2979})(h/a)^{1.3590} \quad (10)$$

This equation is valid for $1.04 \le RG \le 100$ and $0 \le h/a \le 2$ and fit simulated k_{Sc} values within 2.6%. It is worth noting that eq 10 becomes eq 7 for $h/a = 0$, while it converges to eq 5 for $RG \rightarrow \infty$. Finally, the combination of eqs 4 and 10 provides I_{ss} for any sphere cap whose geometric features are within the latter ranges.

Comparison of the Effect of Insulating Shield Thickness on the Steady-State Current of Sphere Caps and Finite Cones. The results obtained above for the sphere caps were compared with those obtained in previous investigations[5,6] with finite cones. Figure 3 shows the normalized steady-state limiting-current values, evaluated by using eq 10 above and eq 20 reported in ref 5 for finite cones, as a function of RG, and for the aspect ratios h/a = 0, 0.5, 1, and 2. One can observe that, although the current decrease with RG is qualitatively similar for both geometries, the sphere caps display larger normalized currents with respect to the corresponding finite cones of same features, i.e., basal radius a and aspect ratio h/a. Moreover, the differences between the steady-state limiting currents for the two geometries become dramatically large when $h/a > 1$. These effects are conceivably related to the larger lateral surface area (A_l) of a sphere cap $A_l = \pi(h^2 + a^2)$ with respect to that of a finite cone $A_l = \pi a(h^2 + a^2)^{1/2}$ of the same a and h/a values.

The current enhancement due to back-diffusion for the various geometries can be better examined by the plots displayed in Figure 3b, where I_{ss}, at a given RG, was divided by the current value corresponding to $RG \rightarrow \infty$ (I_∞). The limiting values, calculated for $RG \rightarrow 1$, are shown in the Table 5. It is evident that, in general, the effect of the back-diffusion is larger at the sphere caps. Moreover, while for a finite cone the maximum current enhancement is ~38%, and changes little with the aspect ratio, for a sphere cap, the current enhancement depends sensibly on h/a and for the biggest electrode examined, an increment of ~60% is found. These aspects should be kept in mind, when geometric parameters of a microelectrode (i.e., the basal radius, or the geometric coefficient k) are obtained through voltammetric measurements, and the assumption of the shape of the microelectrode is made for predicting the steady-state diffusion-limiting currents. In fact, an erroneous choice of the geometry may lead to over- or underestimation of the parameters, which may be well beyond the limits of acceptable experimental error.[5]

Experimental Steady-State Voltammograms of TSSCs. Experimental steady-state limiting currents were obtained from cyclic voltammograms recorded at 1 mV s^{-1} in an aqueous solution of 1 mM $Ru(NH_3)_6^{3+}$ plus 0.1 M KCl as supporting electrolyte. A range of mercury microelectrodes, fabricated on platinum microdisks of 10- and 12.5-μm radius, were investigated. To keep their behavior within the microelectrode properties (i.e., the achievement of a steady state), the aspect ratio of the Hg sphere caps was in the range $0 \le h/a \le 2$. The thin-shielded mercury microelectrodes (i.e., $RG < 5$) displayed, in general, stability, which was as good as that for conventional sphere caps (i.e., $RG \rightarrow \infty$). Figure 4 shows typical voltammograms recorded at a family of TSSCs having different aspect ratios, prepared starting from a thin-shielded disk microelectrode with RG = 1.40, a = 12.8 μm, and b = 17.9 μm. For comparison, a series of CVs obtained with a family of sphere caps fabricated by using a thick-shielded microdisk ($RG > 100$) with a similar basal radius is included. As is evident, in all cases, well-shaped sigmoidal curves with the forward and backward waves almost superimposed are obtained. The achievement of a steady state was assessed by using the criterion of the difference in half-wave potentials ($\Delta E_{1/2}$) observed on the forward and backward waves.[28,32,50,51] At steady state $\Delta E_{1/2}$ should be equal to zero.[28,32,50,51] The analysis of the voltammograms

(50) Zoski, C. G.; Bond, A. M.; Colyer, C. L.; Myland, J. C.; Oldham, K. B. *J. Electroanal. Chem.* **1989**, *263*, 1−21.
(51) Zoski, C. G. *J. Electroanal. Chem.* **1990**, *296*, 317−333.

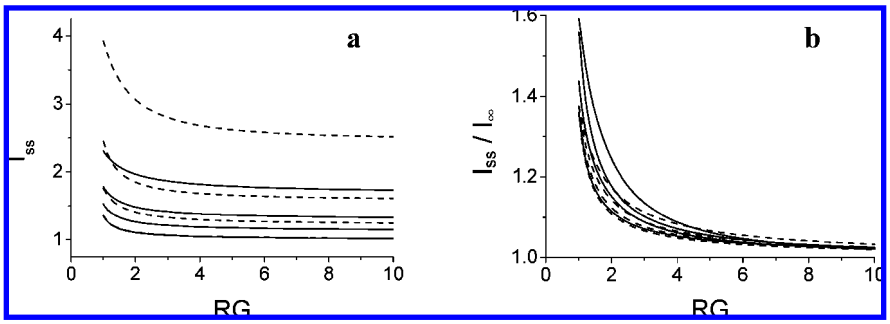

Figure 3. Comparison of (a) normalized steady-state currents, calculated by (—) eq 10 and (– – –) eq 20 in ref 5, respectively, and (b) normalized steady-state currents divided by the current value corresponding to $RG \rightarrow \infty$ (I_∞) for (—) sphere caps and (– – –) finite cones. End to top: $h/a = 0$, 0.5, 1, and 2.

Table 5. Normalized Steady-State Currents of Sphere Cap and Finite Cone Microelectrodes for Different Values of *h/a*, *RG* → 1[a]

	I_{ss}/I_∞	
h/a	*sphere cap*[b]	*cone*[c]
0.0	1.368	1.364
0.5	1.444	1.370
1.0	1.570	1.379
2.0	1.599	1.380

[a] The currents are normalized by I_∞, the current corresponding to $RG \rightarrow \infty$. [b] Calculated from eq 10. [c] Calculated from eq 20 in ref 5.

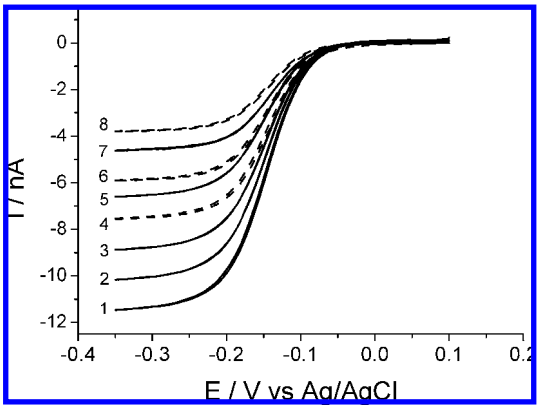

Figure 4. Experimental cyclic voltammograms recorded in 1 mM $Ru(NH_3)_6^{3+}$ + 0.1 M KCl solution; scan rate 1 mV s^{-1} at sphere caps with $RG = 1.40$ (—) and *h/a* equal to (1) =1.61, (2) = 1.42, (3) = 1.05, (5) = 0.55, and (7)= 0; RG = 150 (– – –) and *h/a* equal to (4) = 1.52, (6) = 0.98, and (8) = 0.

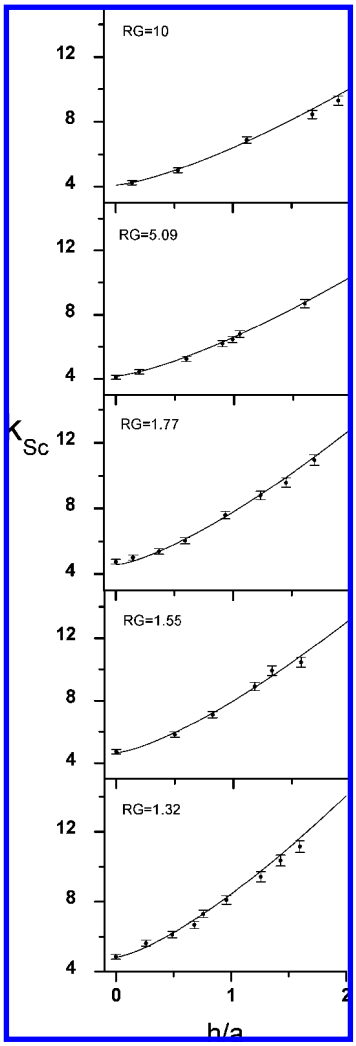

Figure 5. Comparison between experimental (●) and calculated by eq 10 (—) k_{Sc} values for sphere caps of different aspect ratios and the indicated *RG* values.

obtained with the investigated mercury microelectrodes yielded $\Delta E_{1/2}$ values, which varied from 5.0 (±0.5) mV, for rather thick ($RG \geq 10$) shielded electrodes, to 0.5 (±0.2) mV for thinner ones ($RG < 3$). At a given *RG* value, the increase of the aspect ratio led to a slight increase of the hysteresis of the wave. For instance, for the cases shown in Figure 4 ($RG = 1.40$), $\Delta E_{1/2}$ values equal to 0.5, 0.7, 0.9, and 1.5 mV were found for sphere caps with, respectively, $h/a = 0$ (i.e., a disk), 0.5, 1.1, and 1.6. It must be considered that the experimental $\Delta E_{1/2}$ values found here are similar to those reported earlier for thin-shielded disk electrodes.[32] Therefore, the limiting currents found under the adopted experimental conditions should be very close to the true steady-state values.

Returning to the voltammograms in Figure 4, it is also evident that the current plateau increases as *h/a* increases or its *RG* decreases, as predicted by eq 10. Experimental k_{Sc} values obtained from the steady-state limiting current and eq 3 ($D_{Ru(NH_3)_6^{3+}} = 7.0 \times 10^{-6}$ cm^2 s^{-1})[52] for some families of sphere caps, fabricated onto Pt microdisks with various *RG* are shown in Figure 5 with symbols. They were averaged from at least four replicates; the

(52) Sun, P.; Zhang, Z.; Guo, J.; Shao, Y. *Anal. Chem* **2001**, *73*, 5346–5351.

Table 6. Experimental and Theoretical Features for Sphere Cap Mercury Microelectrodes with Different *RG* and *h/a* Values[a]

			a/μm		b/μm			
electrode	I_{exp}/nA	I_{th}/nA	SEM	V	SEM	V	h/μm	h/a
1	5.45	5.53	10.2	10.5 (± 0.2)	20.5	21.8 (± 0.3)	11.2	1.10
2	5.92	5.85	12.7	12.8 (± 0.2)	66.1	64.5 (± 0.3)	13.3	1.05

[a] exp, experimental values; th, theoretical values calculated by eq 10. SEM, obtained by scanning electron microscopy. V, obtained by voltammetry.

error bar reflects the reproducibility, which was in all cases within 1.5%. The solid lines included in Figure 5 represent the corresponding theoretical values calculated by eq 10. In general, a satisfactory agreement between experimental and theoretical values within 3% was found. Comparison between theoretical and experimental normalized steady-state limiting currents for some families of TSSCs are also shown in Figure S2 (see, Supporting Information).

TSSC Parameters from SECM Measurements. Several reports have shown that SECM provides a means for independent validation of the shape and geometric characteristics of a microelectrode obtained from steady-state voltammetry.[16,18,21] The method is based on recording tip current against tip−substrate distance (*d*) plots (approach curves)[18] with respect to either an insulating or a conductive substrate. The fit of experimental and theoretical approach curves provides the quality of the parameters obtained. In a recent paper,[15] the parameters of functions used to predict diffusion-controlled SECM approach curves for sphere cap tips as a function of both *RG* and *h/a* were reported. Thus, in this section, SECM is used to assess the geometric features of two hemispherical mercury microelectrodes fabricated by using platinum microdisks with *RG* equal to 2.0 and 5.1, as determined by using both steady-state voltametry and SEM analysis. The height of the mercury deposit was evaluated from the charge spent during the deposition step, as described in the Experimental Section. Table 6 shows the geometric features of the two mercury microelectrodes obtained by the different procedures. The experimental steady-state limiting currents recorded in 1 mM $Ru(NH_3)_6^{3+}$ and the corresponding theoretical values expected on the basis of eq 10 are included in Table 6. A good agreement within 1.5% between experimental and theoretical values was found. Figure 6 shows typical approach curves obtained with the two mercury microelectrodes (symbols) in a 1 mM $Ru(NH_3)_6^{3+}$ solution. The current against distance plots are normalized for the current in the bulk solutions. As is evident, the fitting is quite good for both insulating and conducting substrates. This result therefore confirms the validity of the tip shape and size obtained by steady-state voltammetry.

CONCLUSIONS

In this paper, the effect of the insulating shield thickness on the steady-state diffusion-limiting currents of sphere cap microelectrodes has been examined in detail. In particular, it has been verified that the current increases by decreasing the *RG* or by increasing the *h/a* parameter, similarly to the case of finite cones with thin shields. An approximate analytical equation has also been derived for predicting the steady-state diffusion-limiting currents at sphere cap microelectrodes of various aspect ratios and

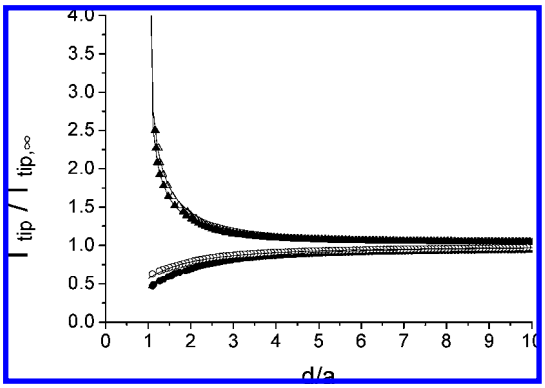

Figure 6. Experimental (symbols) and theoretical (solid lines) approach curves for hemispherical mercury microelectrodes with *RG* = 2 (△) positive and (○) negative feedback, and *RG* = 5(▲) positive and (●) negative feedback.

thickness of the insulating sheath. This equation was derived from simulated data obtained by using the finite difference model employed for analogous predictions at microdisks. The theoretical results were compared with experimental values obtained with a range of mercury microelectrodes, fabricated by coating platinum disk microelectrodes with liquid mercury, using cyclic voltammetry at 1 mV s^{-1} in $Ru(NH_3)_6^{3+}$ aqueous solutions. With very thin-shielded mercury microelectrodes (i.e., *RG* < 3), the voltammograms recorded displayed almost retraceable sigmoidal waves; $\Delta E_{1/2}$ was in the range 0.5 −1.5 mV, indicating a faster achievement of steady-state conditions. This is a consequence of the additional flux due to diffusion from behind the plane of the electrode. These aspects may be useful in stripping analysis, when the preconcentration step is performed under quiescent conditions. In fact, the enhanced flux, associated with a faster achievement of a steady state, may favor a larger metal accumulation within the mercury film, ultimately providing a higher sensitivity in the measurements.

ACKNOWLEDGMENT

The financial support from the Italian Ministry of the University and Research (MUR) is gratefully acknowledged.

SUPPORTING INFORMATION AVAILABLE

Simulation model, definition of the simulation parameters. and Appendix. This material is available free of charge via the Internet at http://pubs.acs.org.

Received for review August 1, 2007. Accepted October 22, 2007.

AC701631Y